NAVAL POSTGRADUATE SCHOOL

MONTEREY, CALIFORNIA

THESIS

LOW BANDWIDTH MATCHED-ILLUMINATION RADAR TRANSMITTER-RECEIVER DESIGN FOR CERTAIN WIDEBAND TARGETS

by

Asaf Berger

September 2019

Thesis Advisor:	Ric Romero
Second Reader:	David C. Jenn

THIS PAGE INTENTIONALLY LEFT BLANK

REPORT DOCUMENTATION PAGE			*Form Approved OMB No. 0704-0188*

1. AGENCY USE ONLY *(Leave blank)*	**2. REPORT DATE** September 2019	**3. REPORT TYPE AND DATES COVERED** Master's thesis

4. TITLE AND SUBTITLE
LOW BANDWIDTH MATCHED-ILLUMINATION RADAR TRANSMITTER-RECEIVER DESIGN FOR CERTAIN WIDEBAND TARGETS

5. FUNDING NUMBERS
REN2X

6. AUTHOR(S) Asaf Berger

7. PERFORMING ORGANIZATION NAME(S) AND ADDRESS(ES)
Naval Postgraduate School
Monterey, CA 93943-5000

8. PERFORMING ORGANIZATION REPORT NUMBER

9. SPONSORING / MONITORING AGENCY NAME(S) AND ADDRESS(ES)
N/A

10. SPONSORING / MONITORING AGENCY REPORT NUMBER

11. SUPPLEMENTARY NOTES The views expressed in this thesis are those of the author and do not reflect the official policy or position of the Department of Defense or the U.S. Government.

12a. DISTRIBUTION / AVAILABILITY STATEMENT	**12b. DISTRIBUTION CODE**
Approved for public release. Distribution is unlimited.	A

13. ABSTRACT (maximum 200 words)

Traditional radar waveform design relies on the point target assumption; however, targets in general have complex and extended responses, which have been shown in cognitive radar studies. Matched illumination waveforms for these types of targets yield higher probability of detection than traditional wideband radar waveforms. There are some challenges to implementing matched waveforms in a practical radar system, such as requirements for high bandwidth to measure target response. In this work, we tackle some of these challenges. We also introduce a low-cost radar system design by taking a novel approach to integrating the multiple-low-rate samplers (MLRS)-based receiver with matched illumination waveforms for specific targets. This design approach is tested using drones as targets in an anechoic chamber for several angles and frequencies. Results show that the probability of detection for our integrated low sampling rate-matched waveform design is higher than traditional radar wideband waveform and similar to a full-bandwidth matched waveform sampled by a traditional high sampling rate receiver.

14. SUBJECT TERMS	**15. NUMBER OF PAGES**
radar, cognitive radar, low-rate sampling, ADC, detection, RCS measurements, wide-band target response	61
	16. PRICE CODE

17. SECURITY CLASSIFICATION OF REPORT	**18. SECURITY CLASSIFICATION OF THIS PAGE**	**19. SECURITY CLASSIFICATION OF ABSTRACT**	**20. LIMITATION OF ABSTRACT**
Unclassified	Unclassified	Unclassified	UU

NSN 7540-01-280-5500

Standard Form 298 (Rev. 2-89)
Prescribed by ANSI Std. 239-18

THIS PAGE INTENTIONALLY LEFT BLANK

Approved for public release. Distribution is unlimited.

LOW BANDWIDTH MATCHED-ILLUMINATION RADAR TRANSMITTER-RECEIVER DESIGN FOR CERTAIN WIDEBAND TARGETS

Asaf Berger
Major, Israel Defence Forces
BSc in Physics, Tel Aviv University, 2009
BSc in Electrical Engineering, Tel Aviv University, 2009

Submitted in partial fulfillment of the
requirements for the degree of

MASTER OF SCIENCE IN ENGINEERING SCIENCE
(ELECTRICAL ENGINEERING)

from the

NAVAL POSTGRADUATE SCHOOL
September 2019

Approved by: Ric Romero
Advisor

David C. Jenn
Second Reader

Douglas J. Fouts
Chair, Department of Electrical and Computer Engineering

THIS PAGE INTENTIONALLY LEFT BLANK

ABSTRACT

Traditional radar waveform design relies on the point target assumption; however, targets in general have complex and extended responses, which have been shown in cognitive radar studies. Matched illumination waveforms for these types of targets yield higher probability of detection than traditional wideband radar waveforms. There are some challenges to implementing matched waveforms in a practical radar system, such as requirements for high bandwidth to measure target response. In this work, we tackle some of these challenges. We also introduce a low-cost radar system design by taking a novel approach to integrating the multiple-low-rate samplers (MLRS)-based receiver with matched illumination waveforms for specific targets. This design approach is tested using drones as targets in an anechoic chamber for several angles and frequencies. Results show that the probability of detection for our integrated low sampling rate-matched waveform design is higher than traditional radar wideband waveform and similar to a full-bandwidth matched waveform sampled by a traditional high sampling rate receiver.

THIS PAGE INTENTIONALLY LEFT BLANK

Table of Contents

THIS PAGE INTENTIONALLY LEFT BLANK

List of Figures

List of Tables

THIS PAGE INTENTIONALLY LEFT BLANK

List of Acronyms and Abbreviations

ADC	analog to digital converter
ARSENL	advanced robotic systems engineering laboratory
AWG	arbitrary waveform generator
AWGN	additive white Gaussian noise
CRr	cognitive radar
CST	computer simulation technology
dB	decibel
ESV	energy spectral variance
ESD	energy spectral density
EM	electromagnetic
MI	mutual information
MLRS	multiple-low-rate samplers
Pd	probability of detection
PFA	probability of false alarm
PSD	power spectral density
PSV	power spectral variance
PWSV	probability-weighted spectral variance
PWE	probability-weighted energy
RCS	radar cross section

SDR software defined radio

SNR signal-to-noise ratio

UWB ultra-wideband

VSA vector signal analyzer

Acknowledgments

First, I would like to thank my thesis advisor, Prof. Ric Romero. His combination of deep theoretical knowledge and hands-on experience is rare to find, and I am grateful for the opportunity to work and learn from him. This would not have been possible without his guidance and support. I would also like to acknowledge Prof. David Jenn as the second reader of this thesis. I have learned a lot from his classes and found them to be very useful when I was working on this thesis.

I thank Mr. Bob Broadston, ME5 Ben Muwei Bey from the Republic of Singapore Air Force, and LT Heitor Albuquerque from the Brazilian Navy. The anechoic chamber experiment was a team effort and I would not have had the data needed for this research without their help.

Finally, I would like to express my gratitude to my wife for her support, patience and understanding along this journey. Thank you for believing in me and always pushing me forward.

THIS PAGE INTENTIONALLY LEFT BLANK

CHAPTER 1:
Introduction

1.1 Motivation

Traditionally, in terms of transmit waveforms, radar designers utilize the point target assumption, which assumes that a target has an approximately flat wideband frequency response. In general, however, targets have far more complex responses. In examining target responses, we can see that some frequencies have higher amplitudes than others. Studies in cognitive radar (CRr) suggest that a better waveform design approach is to take into account the actual target response. This technique is called matched-illumination waveform, which can greatly improve probability of detection [1]-[3].

There are several challenges to using matched illumination waveform in a radar system. One such challenge is the requirement of some knowledge of the target response. In this work, we address the case of a known target response. We also treat the case where the target aspect angle changes with respect to the radar. The exact angle may not be known or may be known with some deviation. Another challenge is the high bandwidth required to implement a matched illumination waveform. Matched illumination potentially requires high-bandwidth waveform which is designed to take advantage of the full target response bandwidth [1]-[4]. Although a high bandwidth radar waveform has many advantages, such as high range resolution [5] and low probability of interception [6], it forces a more complicated system design and a large sampling rate, which imposes the use of an expensive analog to digital converter (ADC) and other hardware elements.

In this work, we try to address these challenges to ease some of the requirements for matched illumination waveform implementation and present a design approach that can lead to a future low-cost detection system.

1.2 Background

Matched Illumination Waveforms

Matched illumination waveforms, or matched waveforms, are radar transmit waveforms designed to match the target response [1]. Traditional radar waveforms are usually designed without full consideration of the target response. In other words, a target is assumed to have a flat wideband target response. Since the received radar signal is the result of convolution of the transmit waveform and the target impulse response, some prior knowledge of the target response can help to design a matched waveform with better detection performance for certain targets [2]. There are two popular metrics to derive matched illumination waveforms [1]. The first is signal-to-noise ratio (SNR)-based matched waveform, which is designed to maximize target return signal-to-noise ratio, and the second is mutual information (MI)-based waveform, which is a metric from information theory, and is designed to maximize MI between the target and received signal.

Multiple Low-Rate Samplers (MLRS)

Many methods exist for low-rate sampling of wideband signals. For example, compressive sensing is one technique that relies on a signal that is sparse in some domain [7]. Another method for low-rate sampling is undersampling, which relies on different sampling rates to resolve ambiguity [8]. These methods may require high computational complexity and latency. For our research we choose another approach of transmitting and receiving a signal through small bandwidth channels. This is not exactly a sub-Nyquist technique in a sense that we do not reconstruct the received signal in its full bandwidth. The potential capability of a CRr to sample part of a wideband transmit waveform, to detect, and to reconstruct the signal with little to no degradation in performance was shown in [9]. In addition, with the right choice of subbands or channels and corresponding filters, we can use multiple low-rate samplers to sample a wideband signal with similar detection performance as compared to a wideband receiver that captures the full bandwidth of the signal.

1.3 Objective

The contribution of this work is a novel approach of integrating matched-illumination waveforms to a MLRS-based receiver. Low-rate sampling has some advantages over wideband

sampling, such as cost reduction, lower computational complexity, a smaller size, and lower cooling requirements, which can be used in the future as a building block for a low-cost detection system. Design performances are simulated using target responses measured in an anechoic chamber. We also analyze the effect of optimal filter allocation and large angle deviation on detection performance.

1.4 Thesis Organization

This thesis is organized as follows. An introduction and previous work are described in Chapter 1. Matched illumination waveform design using multiple low-rate samplers, an algorithm for selection of optimal set of channel frequencies, and waveform design for both SNR-based and MI-based matched waveforms are presented in Chapter 2. The target model and target angular deviation are described in Chapter 3. Targets response measurements taken in an anechoic chamber, a description of a method for measuring wideband target response using coherent integration, and deconvolution for extracting target response from the received signal are described in Chapter 4. Results of waveform design performance using Monte Carlo simulations with measured target responses from an anechoic chamber are presented in Chapter 5. Summary, conclusions, and recommendations are discussed in Chapter 6.

THIS PAGE INTENTIONALLY LEFT BLANK

CHAPTER 2:
Matched Illumination for Multiple Low-Rate Samplers

We use the method of MLRS from [9], [10], which avoids a high sampling rate and yet maintains high detection performance by utilizing prior knowledge of the target response. A small number of receiver subchannels are used. In addition to MLRS from [9], in this research, the transmit waveform is also matched to the receiver subchannels with the use of SNR and MI matched illumination waveforms [1], [2]. The receiver architecture is shown in Figure 2.1. For simulation purposes, we use perfect bandpass filters with a gain of 1 in the passband frequencies and a gain of 0 outside those frequencies. Although in theory these filters have an infinite time response, we use a finite time response and assume that most of the energy is confined to a finite time interval and only negligible energy is transmitted and received outside the bandpass frequencies.

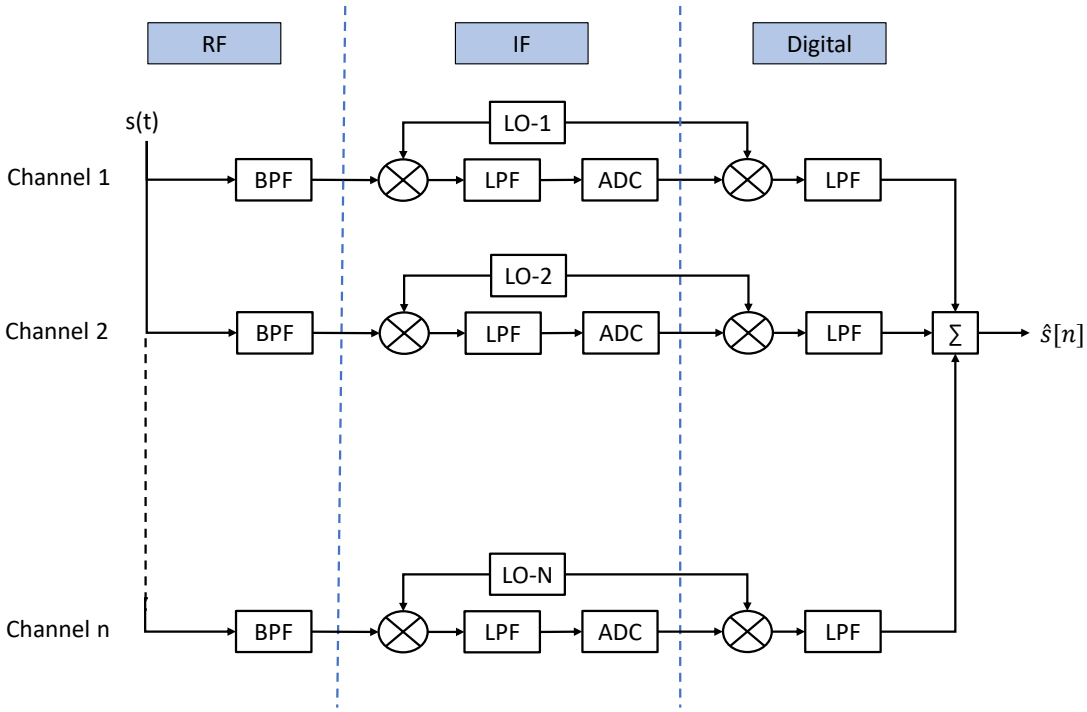

Figure 2.1. Multiple low-rate samplers based receiver architecture.

2.1 Applying MLRS to Matched Illumination Waveforms

Applying MLRS to SNR Based Waveform

SNR-based waveform for target detection in noise was presented in [1], [2], which ensured maximum SNR at the receiver output. Let $\mathbf{h}(t)$ be the baseband target impulse response with Fourier transform $\mathbf{H}(f)$. In this work, we may treat $\mathbf{h}(t)$ to be a deterministic signal or a random signal with a few realizations corresponding to our target measurements in various angles, which is discussed in more detail in Chapter 3. We assume zero-mean noise with a power spectral density (PSD) of $S_{nn}(f)$. We let $x(t)$ be the baseband transmit waveform with a Fourier transform $X(f)$ and duration T. Let $W(f) = \sum_{i=1}^{n} B_i(f)$, where n is the number of subchannels and each filter is defined by

$$B_i(f) = \begin{cases} 1 & f_{low_i} < f < f_{high_i} \\ 0 & \text{otherwise} \end{cases}, \tag{2.1}$$

where i is the filter index and f_{low_i} and f_{high_i} are the filter cut-off frequencies. The filter $B_i(f)$ has a bandwidth of B_i, and the total bandwidth for the filter set $W(f)$ is W. In other words, the total bandwidth of the subchannel filters is given by

$$W = \sum_{i=1}^{n} B_i. \tag{2.2}$$

Under the assumption of perfect filter response, the transmit waveform energy is

$$E_x = \int_{-\infty}^{+\infty} |W(f)||X(f)|^2 \, \mathrm{d}f. \tag{2.3}$$

We define the target spectral variance as,

$$\sigma_H^2(f) = \mathrm{E}[|\mathbf{H}(f) - \mu_H(f)|^2], \tag{2.4}$$

where $\mu_H(f)$ is the mean frequency response. From [1], [2], the SNR is given by

$$\text{SNR} = \int_{-\infty}^{+\infty} \frac{\sigma_H^2(f)|X_(f)|^2}{S_{nn}(f)}\,\mathrm{d}f. \tag{2.5}$$

In our case, since we are practically bandlimited, the SNR is approximately given by

$$\text{SNR} \approx \int_{-\infty}^{+\infty} \frac{\sigma_H^2(f)|X(f)|^2|W(f)|^2}{S_{nn}(f)}\,\mathrm{d}f. \tag{2.6}$$

The transmit waveform is found using [1] and is given by

$$\lambda_{max}x(t) = \int_{-T/2}^{T/2} x(\tau)R_g(t-\tau)\,\mathrm{d}\tau, \tag{2.7}$$

where the kernel is $R_g(t)$ is defined by

$$R_g(t) = \int_W \frac{\sigma_H^2(f)}{S_{nn}(f)} e^{j2\pi ft}\,\mathrm{d}f. \tag{2.8}$$

Incorporating the filters, the kernel becomes

$$R_g(t) = \int_{-\infty}^{+\infty} \frac{\sigma_H^2(f)|W(f)|^2}{S_{nn}(f)} e^{j2\pi ft}\,\mathrm{d}f. \tag{2.9}$$

Defining

$$G(f) = \frac{\sigma_H^2(f)|W(f)|^2}{S_{nn}(f)}, \tag{2.10}$$

we can see that the kernel $R_g(t)$ is the inverse Fourier transform of $G(f)$. From [1], the SNR for this waveform is given by

$$\text{SNR} = \lambda_{max}E_x. \tag{2.11}$$

To compute the transmit waveform $x(t)$, we endeavor to find a filter of the form $W(f) = \sum_{i=1}^{n} B_i(f)$. Since we are looking for a design approach that leads to a simple low-cost system,

we can assume n is a small number. This is because a system with many subchannels is likely to be complex and expensive, which is the very issue we are trying to solve. For simplicity, we assume that the subchannel bandwidth B_i is the same for all filters and is equal to B. Our purpose is to determine the optimal allocation of the filters in the frequency domain.

Assuming E_x is the energy constraint, we can divide the energy between the different filters in a way that the total energy is preserved. In other words, no matter the filter allocation, the total energy is constant. By solving (2.7) we form the transmit waveform $x(t)$, which satisfies the energy constraint (2.3).

We can see from (2.11) that the SNR is directly proportional to λ_{max}. The bandwidth impact on the eigenvalues was discussed in [11]; however, in our case, it is simpler to find the optimal filter allocation by generating $R_g(t)$ for all the different combinations of filter allocation. The number of combinations is a relatively low under the assumption of a small number of filter channels.

The optimal selection process is shown in Figure 2.2. The optimal filter set $W_{opt}(f)$ is the set $W(f) = \sum_{i=1}^{n} B_i(f)$ that maximizes the maximum eigenvalue λ_{max} of the kernel $R_g(t)$ for this specific set of filters. The filter gain is equal for every subchannel in the filter set. In our algorithm, we generate all filter allocation combinations. For each combination, we first

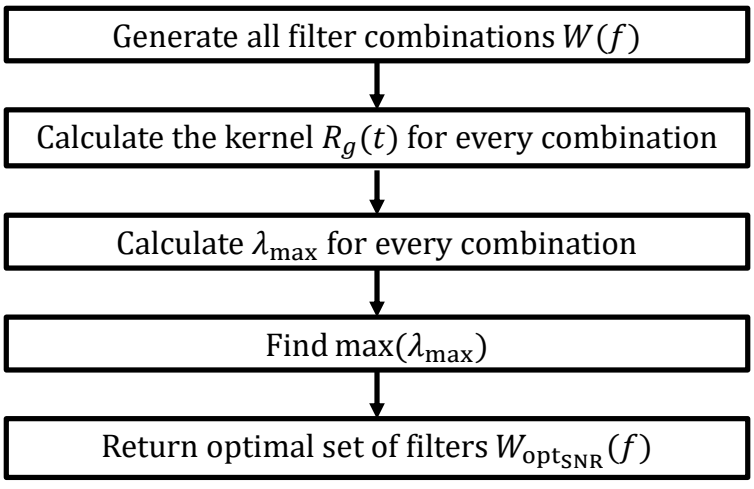

Figure 2.2. Optimal filter set selection process for SNR-based waveform.

compute $R_g(t)$ with (2.9). Then, we can solve (2.7) to produce the transmit waveform $x(t)$ and the maximum eigenvalue λ_{max}. The optimal filter set $W_{opt}(f)$ is the filter combination that yields the highest value of λ_{max}.

The return signal $s(t)$ is a convolution of the transmit waveform $x(t)$ with the target impulse response $\mathbf{h}(t)$ and is given by

$$s(t) = x(t) * \mathbf{h}(t). \tag{2.12}$$

The receiver output $y(t)$ is the convolution of return signal $s(t)$, the filter set impulse response $W_{opt}(t)$, and the optimal receiver filter $r(t)$

$$y(t) = r(t) * W_{opt}(t) * s(t) \tag{2.13}$$

where $W_{opt}(t)$ is the Fourier transform of $W_{opt}(f)$. In other words,

$$y(t) = r(t) * W_{opt}(t) * x(t) * \mathbf{h}(t). \tag{2.14}$$

The optimal waveform/receiver-filter pair that maximizes the SNR of the output signal $y(t)$ at a time t_0, was reported in [1], where the receiver filter frequency response is

$$R(f) = \frac{\kappa H(f) X(f) e^{-j2\pi f t_0}}{S_{nn}(f)} \tag{2.15}$$

and κ is a constant.

Applying MLRS to Mutual Information Based Waveform

MI-based waveform for target estimation in noise was presented in [1], [2], where the waveform ensures maximum MI. We would like to select a waveform $x(t)$ and optimal bandpass filter set $W(f)$ to maximize the MI between the target response $\mathbf{h}(t)$ and the receiver measurement signal $y(t)$. If the target is a stochastic target with energy spectral variance (ESV) of $\sigma_H^2(f)$, then the output ESV is given by

$$\sigma_Y^2(f) = \sigma_H^2(f)|X(f)|^2|W(f)|^2. \tag{2.16}$$

T_y is the measurement duration and it is the sum of transmit time T and the target response time T_h. We can define the time-average power spectral variance (PSV) for $y(t)$ as

$$\Upsilon_y(f) = \frac{\sigma_Y^2(f)}{T_y} = \frac{\sigma_H^2(f)|X(f)|^2|W(f)|^2}{T_y}, \tag{2.17}$$

and the time-average PSV for $h(t)$ is

$$\Upsilon_h(f) = \frac{\sigma_H^2(f)}{T_h}, \tag{2.18}$$

where T_h is the target response time (assuming finite duration). From [2], in the absence of clutter (noise-only scenario), the approximate information rate is

$$I(y(t); \mathbf{h}(t)|x(t)) = \int_W \ln\left[1 + \frac{\Upsilon_y(f)}{S_{nn}(f)}\right] \mathrm{d}f = T_y \int_W \ln\left[1 + \frac{\sigma_H^2(f)|X(f)|^2}{S_{nn}(f)(T + T_h)}\right] \mathrm{d}f. \tag{2.19}$$

Assuming $T \gg T_h$, we get

$$I(y(t); \mathbf{h}(t)|x(t)) = T_y \int_W \ln\left[1 + \frac{\sigma_H^2(f)|X(f)|^2}{TS_{nn}(f)}\right] \mathrm{d}f, \tag{2.20}$$

and we can find $X(f)$ using

$$|X(f)|^2 = \max\left[0, A - \frac{TS_{nn}(f)}{\sigma_H^2(f)}\right] |W(f)|. \tag{2.21}$$

The constant A is defined by the energy constraint

$$E_x = \int_W \max\left[0, A - \frac{TS_{nn}(f)}{\sigma_H^2(f)}\right] \mathrm{d}f. \tag{2.22}$$

Assuming that observation time is approximately equal to the transmission time T, the maximal information is given by [1]

$$I_{max} = T \int_W \max\left[0, \ln\left(A\sigma_H^2\right) - \ln\left(TS_{nn}(f)\right)\right] \mathrm{d}f. \tag{2.23}$$

We can form a waveform using (2.21) while following the constraint of (2.22) for all different combinations of filters $W(f)$ to find the optimal set of filters that provides the maximal I_{max}. The procedure is described in Figure 2.3. This optimal set is used to derive the transmission waveform $X(f)$.

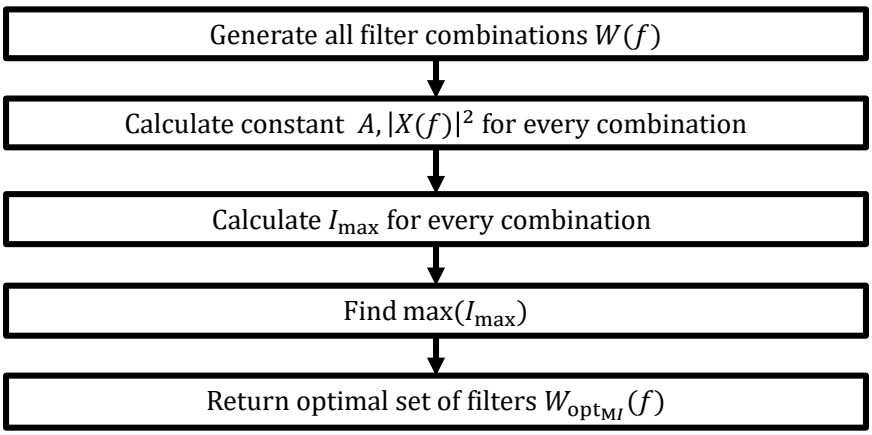

Figure 2.3. Optimal filter set selection procedure for MI-based waveform.

2.2 Probability of Detection

Our work concentrates on detection. Usually the most important measure of performance for a detection system is the probability of detection (P_d) given certain transmission energy and false alarm rate (P_{FA}).

In modern digital radar, detection is deemed after the downconverted signal is sampled using an ADC and is passed through a digital filter called a matched filter. Assuming additive white Gaussian noise (AWGN), the matched filter is designed to maximize the output SNR [12]. The probability of detection is a function of SNR and maximizing SNR also optimizes the probability of correctly detecting a signal within noise; hence, the matched filter is the optimum filter for maximum probability of detection. As shown in Figure 2.4, the transmit waveform $x(t)$ illuminates the target response $h(t)$. The target return is sampled by the ADC yielding the vector signal $\mathbf{s}$, where it is corrupted by noise $\mathbf{n}$. The power of the noise depends on receiver temperature, bandwidth, and noise figure. In signal processing, the sampling time is usually normalized for the signal vectors; thus,

$$\mathbf{y_{in}} = \mathbf{s} + \mathbf{n}. \tag{2.24}$$

Since $\mathbf{s}$ is the return signal from the target, it may formulated to be the convolution of the transmit waveform $\mathbf{x}$ and the target response $\mathbf{h}$ and is given by

$$\mathbf{s} = \mathbf{x} * \mathbf{h}, \tag{2.25}$$

where $\mathbf{x}$ is the vector form of $x(t)$ and $\mathbf{h}$ is the vector form of $h(t)$. To decide if the sample signal contains a target return, the matched filter output is compared to a threshold, and from [13] the detection threshold for a given P_{FA} is

$$\gamma' = \sqrt{\sigma^2 E} Q^{-1}(P_{FA}), \tag{2.26}$$

where Q^{-1} is the inverse Q-function, σ^2 is the noise variance and E is the return signal energy which is given by [14]

$$E = E_s = \mathbf{x}^\dagger \mathbf{R_h} \mathbf{x}. \tag{2.27}$$

$\mathbf{R_h}$ is the autocorrelation matrix of the target response convolution matrix $\mathbf{H_h}$ and is given

by [14]

$$\mathbf{R_h} = \mathrm{E}\left[\mathbf{H_h}^{\dagger} \cdot \mathbf{H_h}\right], \tag{2.28}$$

where E[] again is the expectation value operator[1]. Now the detection threshold can be written as

$$\gamma' = \sqrt{\sigma^2 \mathbf{x}^{\dagger} \mathbf{R_h} \mathbf{x}} Q^{-1}(P_{FA}). \tag{2.29}$$

A simple form of the probability of detection is given by [13]

$$P_D = Q(Q^{-1}(P_{FA}) - \sqrt{\sigma^2 E}), \tag{2.30}$$

but in our work, the probability of detection is given by [3]

$$P_D = Q(Q^{-1}(P_{FA}) - \sqrt{\sigma^2 \mathbf{x}^{\dagger} \mathbf{R_h} \mathbf{x}}). \tag{2.31}$$

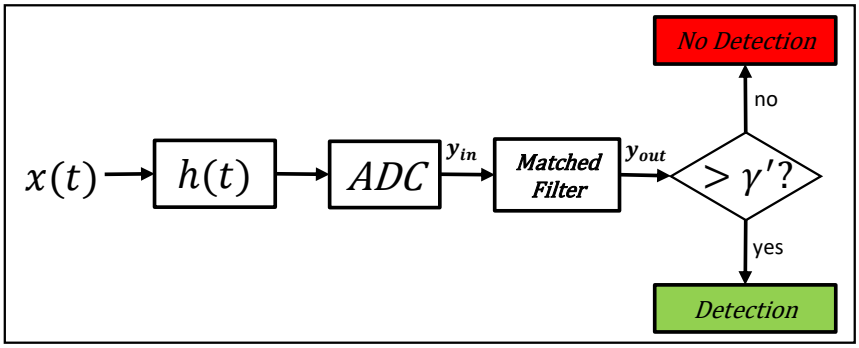

Figure 2.4. Signal detection for signal resulting from convolution of transmit waveform and target response.

[1]Not to be confused with an italicized E which stands for energy value throughout this paper.

THIS PAGE INTENTIONALLY LEFT BLANK

CHAPTER 3:
Target Model

3.1 Target Frequency Response

In traditional radar design, the point target is assumed, which has an approximately flat wideband frequency response. However, for matched illumination waveform, the actual target response needs to be taken into account. SNR-based and MI-based waveforms are matched illumination waveforms designed to match the target response and usually most of the signal energy is transmitted in the higher magnitude frequency bands of the target, which we also referred to as dominant bands [9]. An example of actual target response and its dominant bands are shown in Figure 3.1. The target response comes from a "DJI - M100" drone placed at an azimuth angle of 10° and 0° elevation angle. This target response is extracted from the measurements described in Chapter 4.

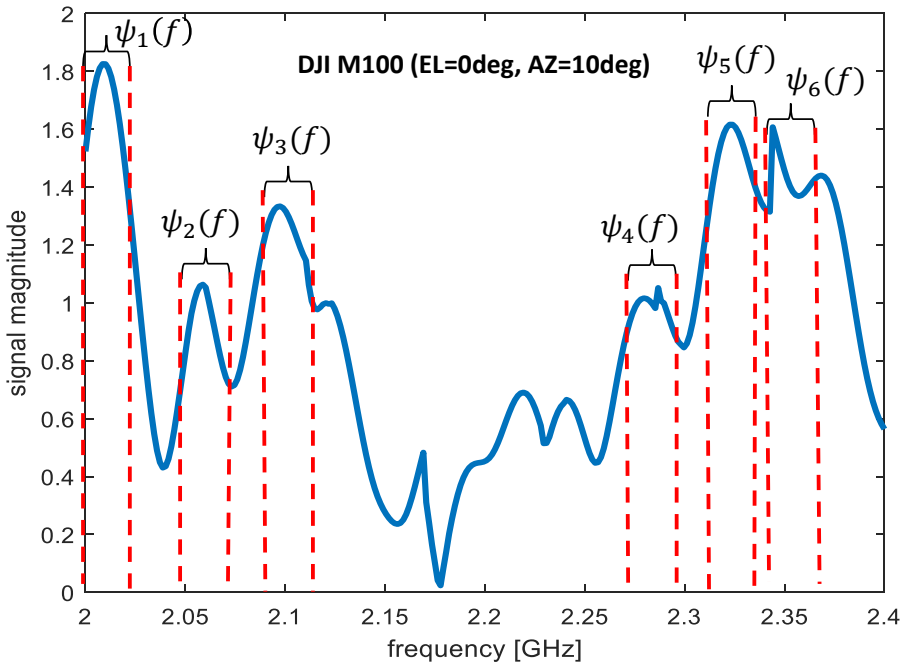

Figure 3.1. Drone target frequency response and dominant bands.

In this work we assume that we know or have measured target responses for all angles of interest as an input for the waveform design process; however, the actual aspect angle of the target to the radar may be unknown. The angular uncertainty can be viewed as uncertainty in the target response, which can be treated as a stochastic target with some spectral variance as described in [14]. This uncertainty needs to be taken into consideration when designing the waveform for a certain angle. In our case, due to equipment limitations (i.e., the turn table used to rotate our targets), the angle differences are large (about 10° angle deviation between measurements). For the large angle deviation, described in Chapter 4, the target responses are almost uncorrelated. As such, we can treat the target response as random with equal probability for every angle.

3.2 Various Angles

When an ensemble of measurements come from M different angles, then a particular angle is given by $\alpha_j(\phi, \theta)$, each with a given probability P_j for a target impulse response $\mathbf{h}_j$. We treat this scenario as an ensemble of known impulse responses as presented in [2], [14]. If we are to calculate detection percentage for this case, we need to decide on a waveform since we have M waveform possibilities. Using the probability weighted energy (PWE) method, the transmit waveform we choose is the probability weighted sum of each angle matched waveform, and is given by [14]

$$\mathbf{x}_{pwe} = \sum_{j}^{M} \sqrt{P_j}\mathbf{q}_j, \tag{3.1}$$

where P_j is the prior probability for the target response $\mathbf{h}_j$, and $\mathbf{q}_j$ is its corresponding matched waveform.

The waveform is scaled to ensure the energy constraint is met and is given by

$$\mathbf{x} = \sqrt{\frac{E_x}{E_{x_{pwe}}}}\mathbf{x}_{pwe}. \tag{3.2}$$

where $E_{x_{pwe}}$ is the resulting energy for (3.1). For the matched filter receiver design (2.14) and (2.15) for an ensemble of responses for various angles, we can also use the probability

weighted target response, which is given by

$$\mathbf{h}_{pwe} = \sum_{j}^{M} \sqrt{P_j}\mathbf{h}_j. \tag{3.3}$$

In our case, we use equal probability for each angle and (3.3) can be written as

$$\mathbf{h}_{pwe} = \frac{\sum_j \mathbf{h}_j}{\sqrt{N}}. \tag{3.4}$$

where M is the number of different angles of interest.

THIS PAGE INTENTIONALLY LEFT BLANK

CHAPTER 4:
Target Response Measurements

To test the theory presented in previous chapters, we desire to utilize target responses from actual physical targets. To acquire the data needed, we developed a method for measuring target response in an anechoic chamber using an arbitrary waveform generator (AWG) for transmission and vector signal analyzer (VSA) as a receiver. For this work we utilize target responses from two drones (Figure 4.1): DJI-M1000 and RiteWing - The Zephyr II , which we borrowed from the NPS advanced robotic systems engineering laboratory (ARSENL). Targets coordinates system are also shown in Figure 4.1. Drone specifications are shown in Table 4.1.

Table 4.1. Drone specifications

Manufacturer	Model	Type	Diameter	Material
RiteWing	Zephyr II	Electric flying wing	142 cm	Mostly foam
DJI	M100	Electric quadcopter	65 cm	Mostly carbon fiber

DJI – M100 RiteWing - The Zephyr II

Figure 4.1. Drones used in the anechoic chamber measurements.

4.1 Anechoic Chamber Measurements Setup

Target response measurements are taken in an anechoic chamber to reduce clutter return and to make it easier to isolate target response from other reflectors. For simplicity, we choose a narrow pulse waveform for transmission. This makes it easier to isolate and process the target return without the need for pulse compression since our objective is not necessarily to increase range resolution. The target is placed on a pedestal approximately 3 meters away from two antennas: one is used for transmission and the other is for reception. We transmit a narrow pulse of 10 ns using an AWG and receive the reflected signal with a VSA operated in I/Q high bandwidth sampling mode. The recorded measurements are processed in MATLAB. The transmit waveform has a bandwidth of 100 MHz. The measurement set-up is illustrated in Figure 4.2.

Since the chamber used is relatively small, the targets chosen for measurements are drones, which are small in size but are still targets of interest in some radar applications. To estimate signal return power, we can use the radar range equation [5]

$$P_{rec} = \frac{P_t G_t G_r \lambda^2 \sigma}{(4\pi)^3 R^4} \tag{4.1}$$

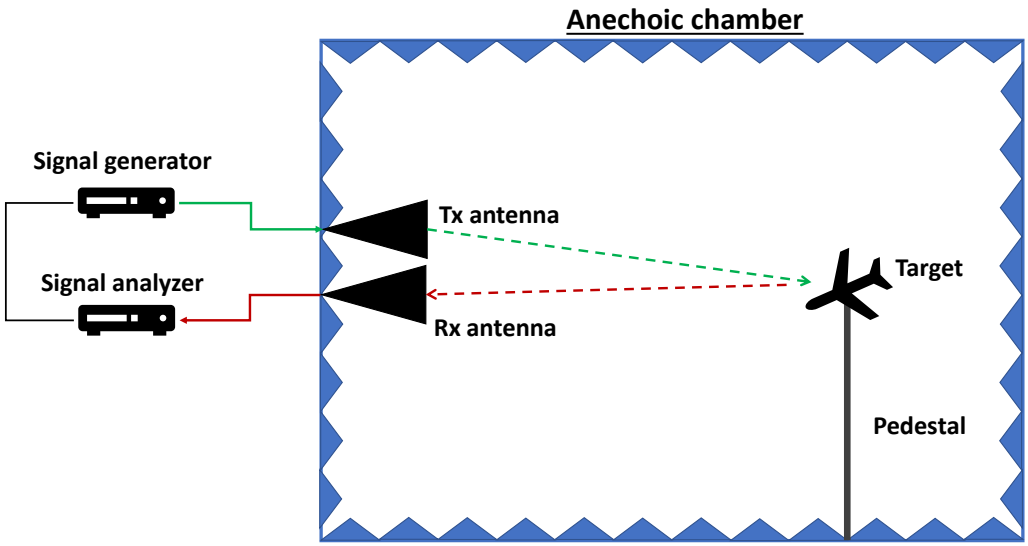

Figure 4.2. Anechoic chamber measurements setup.

where P_t is the transmit power, G_t and G_r are the transmitter and receiver antenna gains, respectively, λ is the signal wavelength, σ is the target radar cross section (RCS), and R is the target distance.

In our chamber, we are limited in the power we are allowed to transmit due to safety regulations. As a result, we choose not to utilize an external power amplifier and instead use the AWG maximum transmit power of 1 Watt. The antennas used are horizontally polarized rigged horn antennas with a gain of 6 dB. Measurements are taken over the frequency range of 2-3 GHz. From [15], a drone RCS in 3-6 GHz is estimated to be between 0.01 m^2 to 0.0001 m^2. Using (4.1), we get an estimate received power of -60 dBm to -80 dBm. The thermal noise level including the receiver noise figure is estimated to be around -75 dBm. This results in an estimated SNR of -5 to 15 dBm.

4.2 Target Response Extraction

There are a couple of post-processing steps to extract target response from the raw measurements. It turns out the return signal is very low (lower than what is estimated), and the measurements are taken using a high bandwidth channel that introduces high noise level. To improve SNR, a coherent integration technique is used. For simplicity, a pulse repetition interval (PRI) is chosen to be an integer number of the wavelength. This method guarantees that each sample has the same phase as the corresponding sample in the next PRI. The output signal $s_{out}[k]$ for the coherent integration for N pulses is

$$s_{out}[k] = \sum_{m=0}^{N-1} s_{in}[k + mPRI], \tag{4.2}$$

where $s_{in}[k]$ is the sampled signal. The coherent integration gain, which is the improvement in the SNR after the integration, is equal to N. If the SNR of the pre-integration signal is $\mathrm{SNR_{in}}$ and $\mathrm{SNR_{out}}$ is the post-integration SNR, then coherent integration gain for N pulses is

$$N = \frac{\mathrm{SNR_{out}}}{\mathrm{SNR_{in}}}. \tag{4.3}$$

In our experiment, after a coherent integration of 5000 pulses, target return signals are amplified and become very noticeable. However, the coherent integration enhances SNR

for every reflected signal, not just the target. Although the measurements are taken in anechoic chamber, there could still be undesired reflections if other objects are in the room. This becomes apparent as initial background measurements found that without a target, a high return signal in the target location is deemed present. This signal is the accumulation of returns, which is most likely signals reflected off the pedestal where a target or antenna is placed for EM measurements. When we take a measurement with a target on top of the pedestal, the pedestal return actually masks the target return. In order to eliminate the pedestal return and possible undesired reflectors that might be in the chamber, we first need to take a recording of the background without a target. This background measurement is used to "clean" a target recording. This is accomplished by lining up all the 5000 returns in phase and performing the coherent integration. The integrated background measurement is subtracted from the integrated target measurement. Illustration of the background subtraction procedure is given in Figure 4.3. Since our target is stationary, in theory, the background signal reduction can eliminate all undesired signals but in practice, equipment limitations, quantization, etc. can, of course, leave some undesired signal residue.

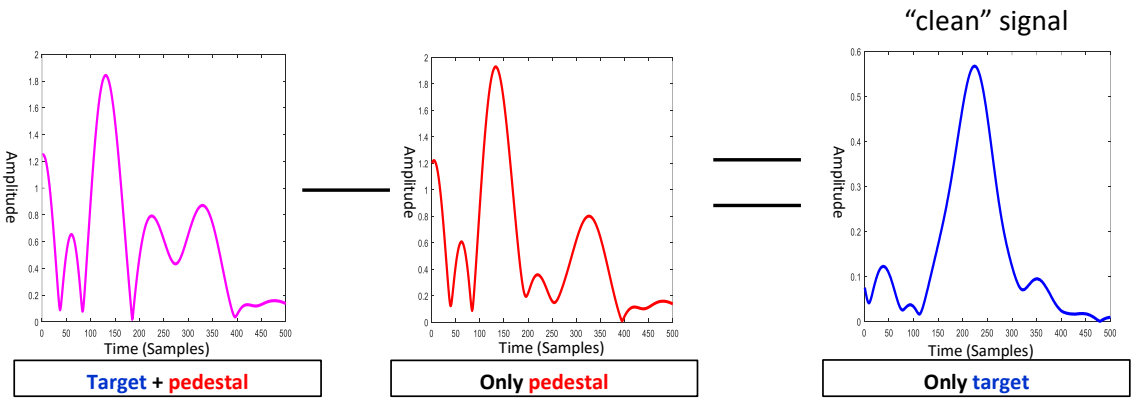

Figure 4.3. Illustration of background subtraction procedure.

Finally, after the coherent integration and extraction of the return echo, we are left with two signals in our recording. The first is $x[k]$, which is the sampled direct transmit signal and the other is $y[k]$ the "cleaned" target return signal. The two signals are separated in time and are easy to distinguish.

The sampled return signal is the result of a convolution of the discrete-time target impulse response $h[k]$ and the sampled transmit waveform $x[k]$. To extract the target impulse response, we need to perform deconvolution operation on the return signal using the transmit waveform. Since convolution of two signals in the time domain corresponds to multiplication in the frequency domain, the two equations that govern the time-frequency transform pairs are given by

$$y[k] = x[k] * h[k] \tag{4.4}$$

and

$$Y(f) = X(f)H(f) \tag{4.5}$$

respectively.

We can extract the target frequency response by dividing the return signal frequency response $Y(f)$ with the transmit waveform frequency response $X(f)$

$$H(f) = \frac{Y(f)}{X(f)}. \tag{4.6}$$

Block diagram of the procedure used for target extraction from the raw measurements is shown in Figure 4.4, assuming coherent integration to background measurements has been performed a priori to the procedure described in Figure 4.4. Interestingly, the procedure we describe here was used in [16] for ultra-wideband (UWB) impulse scattering measurements.

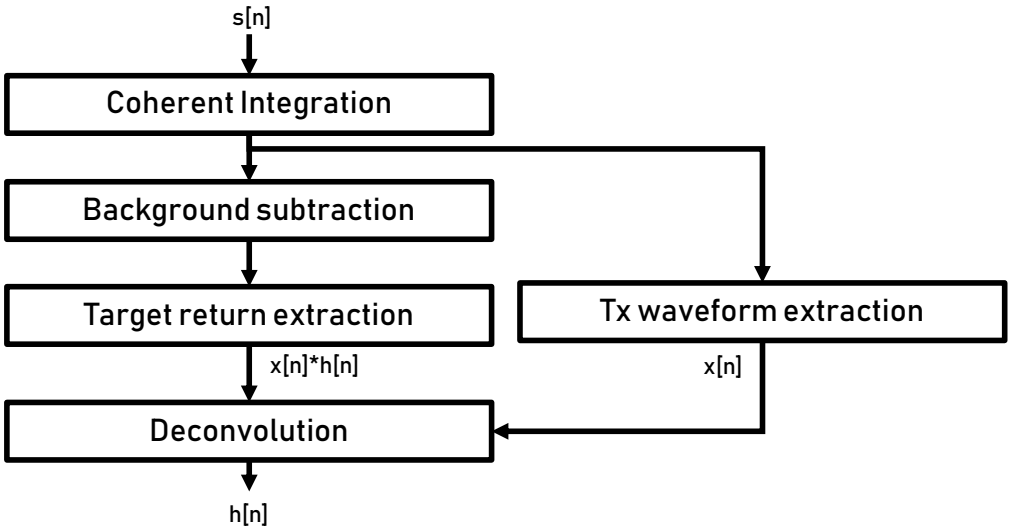

Figure 4.4. Target response extraction procedure.

An example of a target impulse response extracted from the measurements is shown in Figure 4.5 using normalized time sampling. In Figure 4.6, drone energy spectral densities (ESDs) are shown at various azimuth angles with respect to the antennas, which were closely co-located.

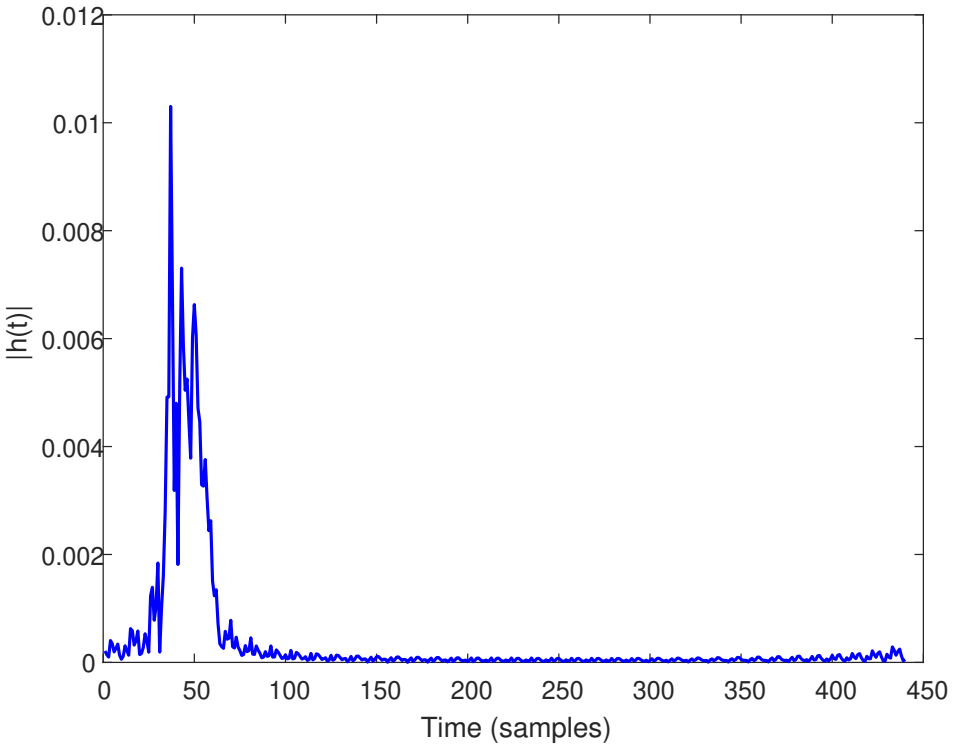

Figure 4.5. ZEPHYRII drone impulse response magnitude at 0° azimuth angle (time domain).

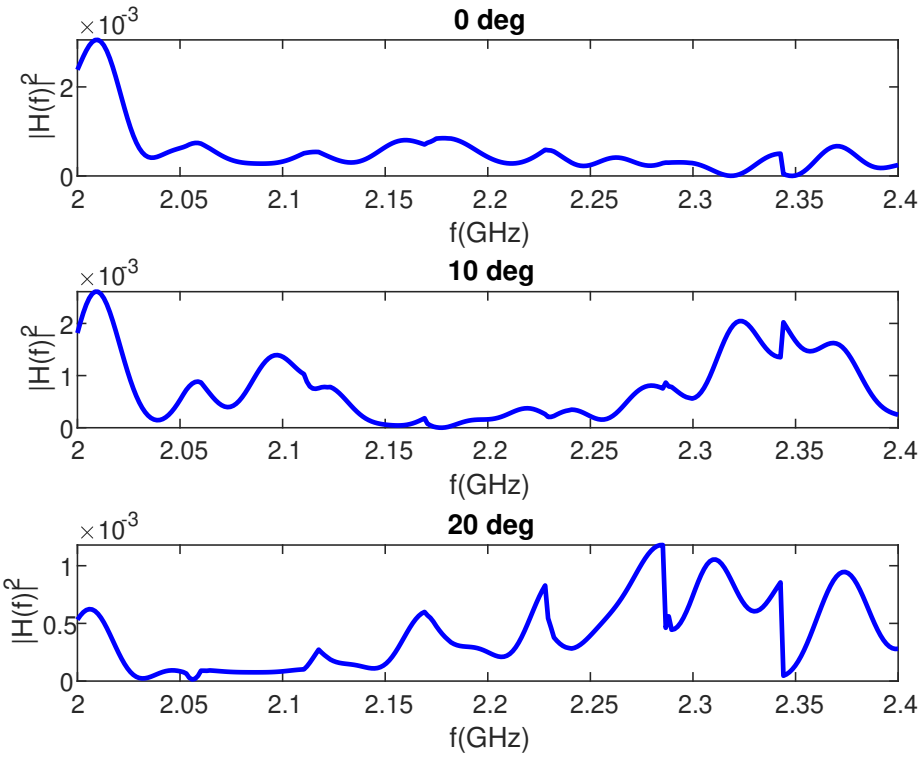

Figure 4.6. DJI-M100 drone ESDs at various azimuth angles. Top: 0° azimuth angle. Middle: 10° azimuth angle. Bottom: 20° azimuth angle.

CHAPTER 5:
Results

The entire signal processing simulation for low-bandwidth matched-illumination radar transmitter-receiver design is tested with the drone measurements presented in Chapter 4 for different number of channels (1-3 channels), different channel bandwidths, and different filter allocation resolutions. In Table 5.1, we show all the different cases used as inputs to the simulation. Probability of detection is computed for increasing transmit energy using Monte Carlo simulations with 1000 trials (per transmit energy) with a fixed $P_{FA} = 0.01$. The theoretical P_d curve is plotted using (2.31). All the measurements are taken with elevation angle of zero degrees with respect to the transmit and receive antennas.

Table 5.1. Simulation inputs

Target type	Azimuth (deg)	Frequency (GHz)	Bands	Filter bandwidth (% of total bandwidth)	Allocation resolution (% of total bandwidth)
Zephyr II	0,10,20	2-3 GHz	1	10%	5,10,15,25%
Zephyr II	0,10,20	2-3 GHz	1	20%	5,10,15,25%
Zephyr II	0,10,20	2-3 GHz	1	30%	5,10,15,25%
Zephyr II	0,10,20	2-3 GHz	2	5%	5%
Zephyr II	0,10,20	2-3 GHz	2	10%	5%
Zephyr II	0,10,20	2-3 GHz	2	15%	5,10%
Zephyr II	0,10,20	2-3 GHz	2	25%	5,10%
Zephyr II	0,10,20	2-3 GHz	3	10%	5%
Zephyr II	0,10,20	2-3 GHz	3	16.67%	5,10%
DJI M100	0,10,20	2-2.4 GHz	1	10%	5,10,15,25%
DJI M100	0,10,20	2-2.4 GHz	1	20%	5,10,15,25%
DJI M100	0,10,20	2-3 GHz	1	30%	5,10,15,25%
DJI M100	0,10,20	2-2.4 GHz	2	5%	5%
DJI M100	0,10,20	2-2.4 GHz	2	10%	5%
DJI M100	0,10,20	2-2.4 GHz	2	15%	5,10%
DJI M100	0,10,20	2-2.4 GHz	2	25%	5,10%
DJI M100	0,10,20	2-2.4 GHz	3	10%	5%
DJI M100	0,10,20	2-2.4 GHz	3	16.67%	5,10%

5.1 Deterministic Target

For the known aspect angle case (i.e., deterministic target), we use each drone measurement as an input for the simulation. For all targets used, the optimal transmitter-receiver design presented in Chapter 2 achieves higher probability of detection in comparison to a wide-band waveform with the same transmit energy. The optimal filter allocation also achieves significantly better results in comparison to a random filter allocation. The Monte Carlo derived P_d curve matches the theoretical curve for all targets tested, as shown by a specific target in a specific angle in Figure 5.1.

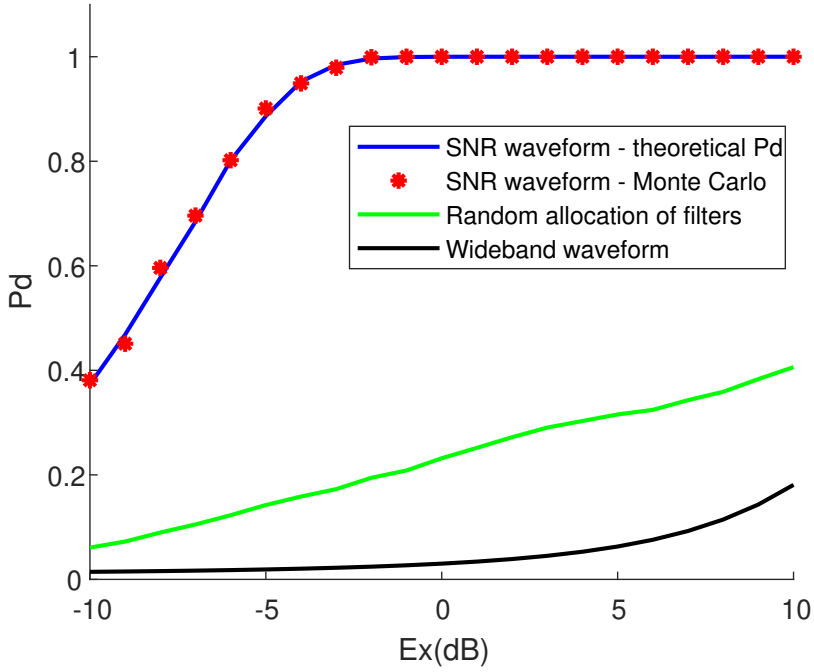

Figure 5.1. Optimal MLRS-SNR based design performance for ZEPHYRII drone at 0° Azimuth in a single band system with 10% bandwidth.

Results for different false alarm rates are shown in Figure 5.2. For the rest of the analysis P_{FA} of 0.01 is used.

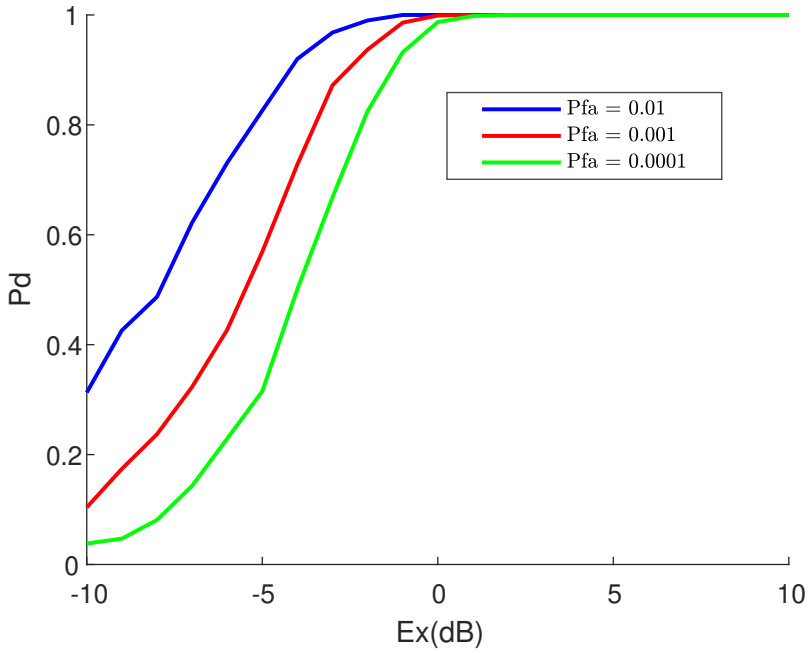

Figure 5.2. SNR waveform detection performance with different $P_{FA}s$ for ZEPHYRII drone at 0° Azimuth in a single band system with a 30% bandwidth.

SNR and MI based waveforms

For the drones used in this work, SNR-based waveforms yield higher probability of detection in comparison to MI-based waveforms with the same transmit energy, as seen in Figure 5.3 for DJI-M100 and ZEPHYRII at 0° azimuth angle.

Channel Bandwidth

Performances of a system with subchannel bandwidths of 10%, 20%, and 30% are compared. As expected, results show an advantage for narrower bandwidths in terms of probability of detection as shown in Figure 5.4. The reason for this outcome is a lower noise level in the narrow bandwidth waveforms.

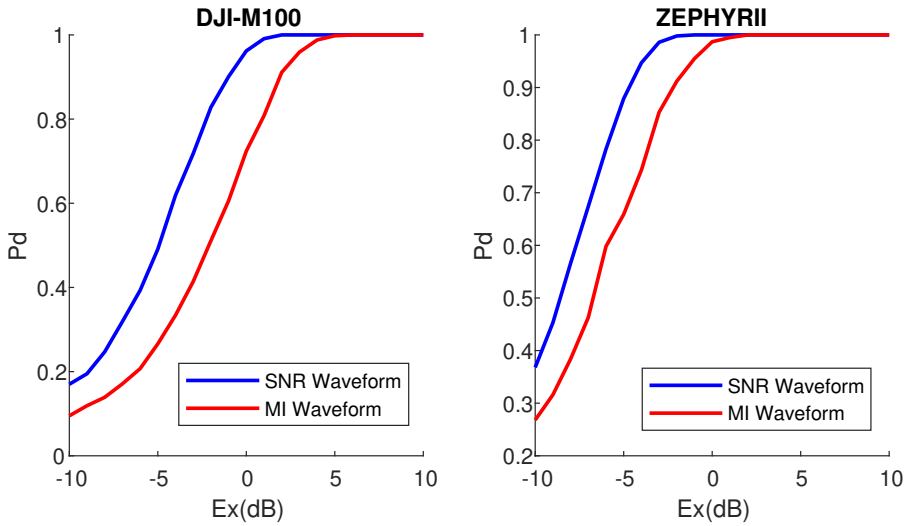

Figure 5.3. Detection performance for low-rate matched-illumination waveforms for a target at 0° azimuth angle. Left: DJI-M100 drone. Right: ZEPHYRII drone.

Number of Channels

The simulation procedure developed in MATLAB is able to execute and find the optimal transmitter-receiver design for up to three channels. We can see in Figure 5.5 that a system with the same total bandwidth but a higher number of channels achieves higher detection performance. The improvement in detection can be explained by more degrees of freedom to select the optimal filter allocation. The two and three channels are able to transmit and receive in frequencies with higher amplitude in the target ESD and are able to avoid lower amplitudes in the target ESD. In this way, the system with more channels (at least up to three) achieves higher probability of detection than a one-channel system with the same total bandwidth.

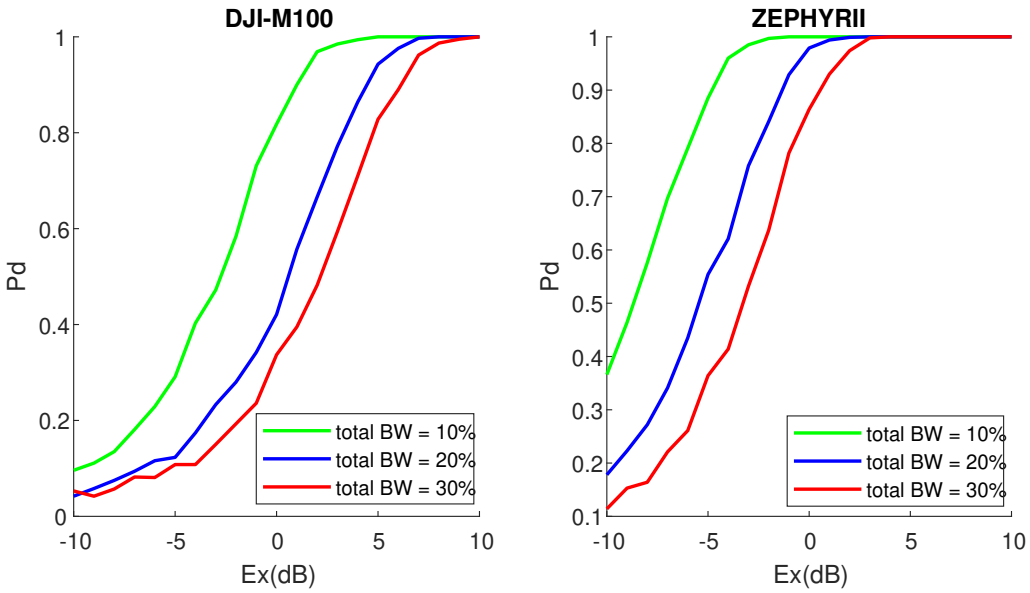

Figure 5.4. Detection performance results utilizing a single frequency band with different percent bandwidths for a target at 0° azimuth angle. Left: DJI-M100 drone. Right: ZEPHYRII drone.

Filter Allocation Resolution

Allocation resolution is the frequency resolution which is used to configure each subchannel center frequency. In order to test the impact of the filter allocation resolution on the detection performance, the filter center frequency allocation resolution is changed from 5% to 25% out of the total bandwidth available. For example, a 5% filter allocation resolution means that we configure the filter center frequency with a frequency step of 5% out of the total bandwidth. We have more possibilities for filter allocation when we use a smaller percentage of filter frequency resolution. For the drones measured, at the resolution of roughly above 15%, the performance of the system starts to degrade, as seen in Figure 5.6.

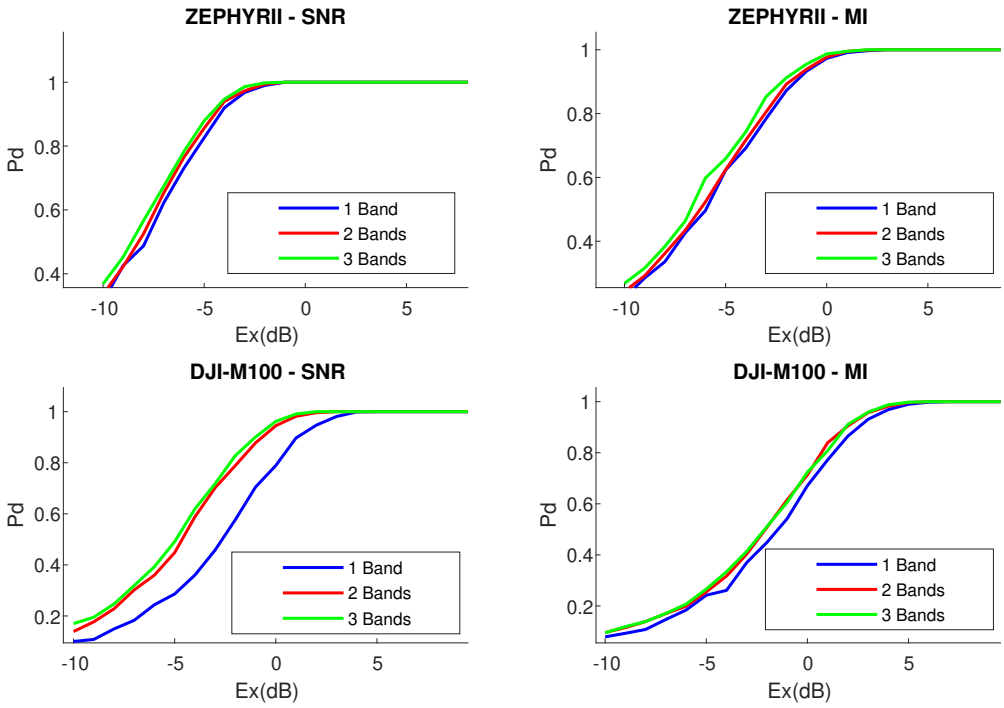

Figure 5.5. Detection performance of different number of channels in a system with a total bandwidth of 30% for target at 0° azimuth angle. Top Left: SNR-Based design for ZEPHYRII drone. Top right: MI-Based design for ZEPHYRII drone. Bottom left: SNR-Based design for DJI-M100 drone. Bottom right: MI-Based design for DJI-M100 drone.

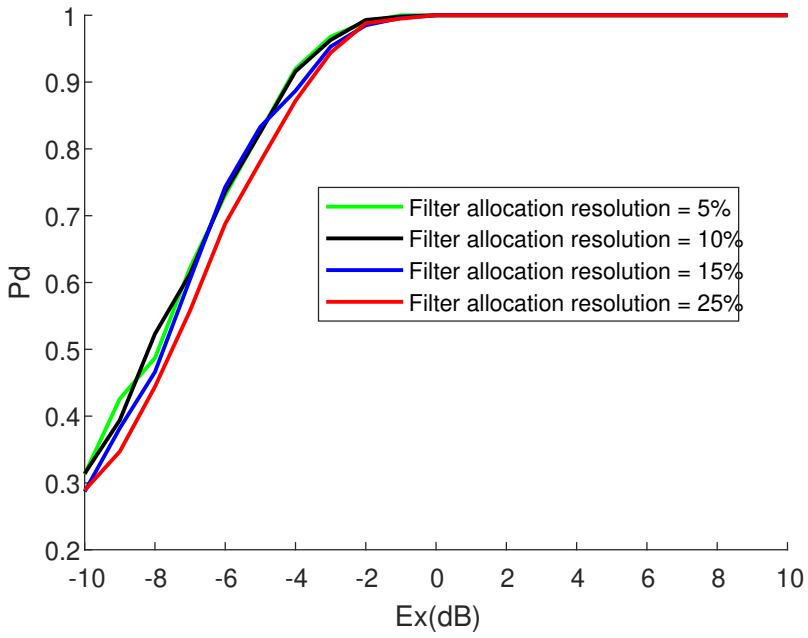

Figure 5.6. Detection performance results utilizing a single frequency band with total bandwidth of 30% and with different filter allocation resolutions, for ZEPHYRII drone at 0° azimuth angle.

5.2 Targets with Various Aspect Angles

In this detection scenario, we assume that the target response can come from three angles with large deviation but the actual realization is unknown a priori in the experiment. In short, the target response comes from a random draw off the three angle set with equal probability for the target azimuth aspect angles of 0°, 10°, and 20°. As expected, the probability of detection in this case, using a PWE matched waveform, is lower than the known angle (deterministic target) case for the same transmit energy. However, the optimal low-rate matched-waveform design performs much better than a random selection of filters. The optimal design also outperforms a wideband design in low-to-moderate energy regions but perform less than or equal to the wideband waveform for a high transmit energy, as shown in Figure 5.7. As observed in [14], a large angle deviation for a target lessens the correlation in the ensemble of target responses. Such low correlation decreases the rate of performance increase in high-energy transmit region for the matched waveforms as compared to the wideband waveform when a target is treated randomly just like in this section. This phenomenon mirrors the RCS behavior of a true target where even a small angle deviation can cause a large change in RCS and thus greatly affecting SNR and detection performance.

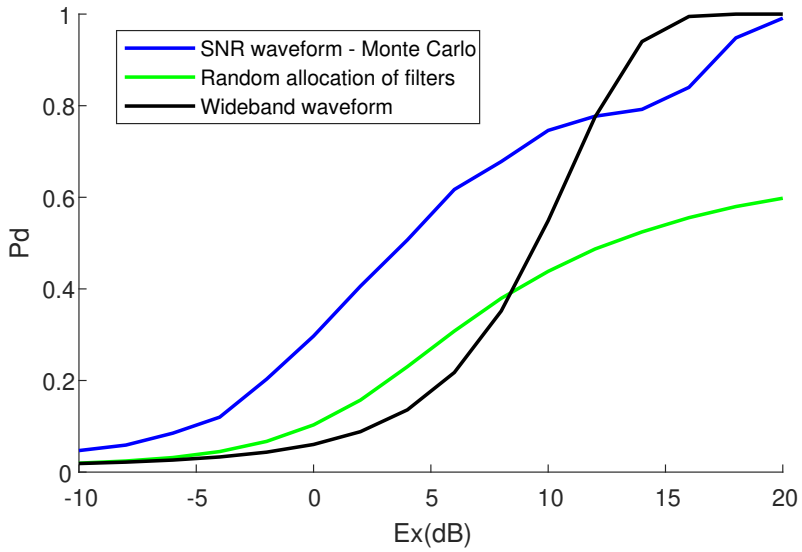

Figure 5.7. Optimal MLRS-SNR based design performance utilizing three frequency bands with total bandwidth of 30% for DJI-M100 at a random angle.

For both drones, the SNR-based waveform performs better than the MI-based waveform, as shown in Figure 5.8. For the case where the number of channels is varied, the results are also similar to the known angle case, as shown in Figure 5.9, where the higher number of channels with the same total bandwidth yield higher probability of detection.

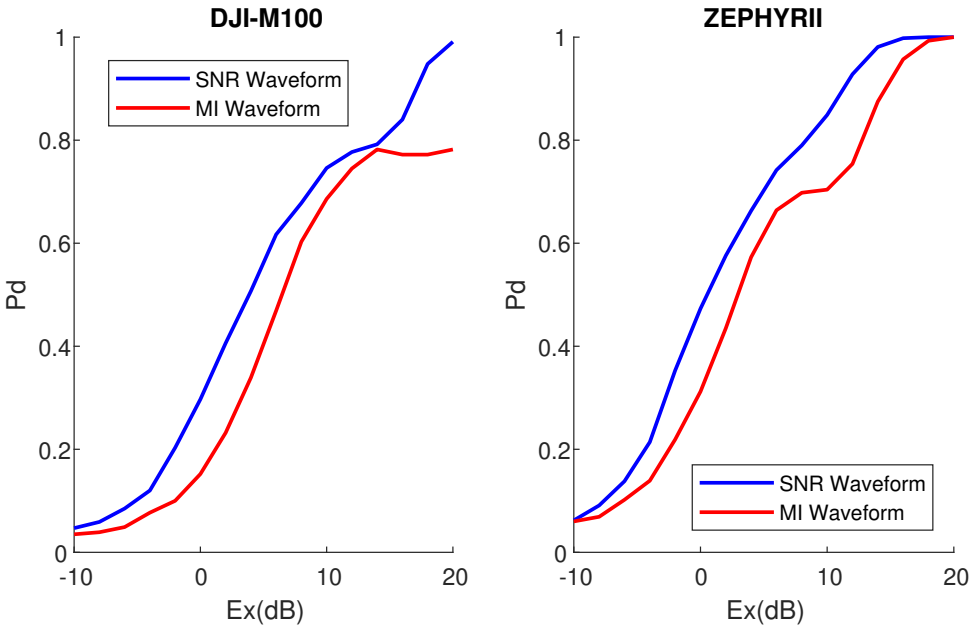

Figure 5.8. Detection performance of SNR and MI-based waveforms utilizing three frequency bands with total bandwidth of 30% for random angle. Left: DJI-M100 drone. Right: ZEPHYRII drone.

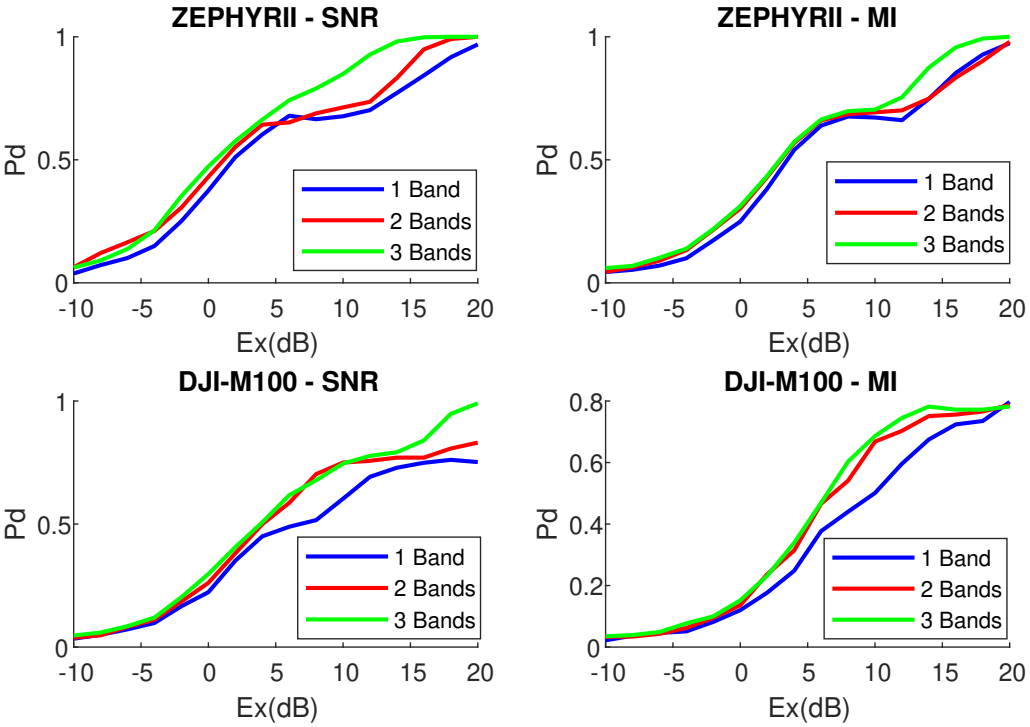

Figure 5.9. Detection performance of SNR and MI-based waveforms utilizing three frequency bands with total bandwidth of 30% and with different number of channels for random angle. Top Left: SNR-Based design for ZEPHYRII drone. Top right: MI-Based design for ZEPHYRII drone. Bottom left: SNR-Based design for DJI-M100 drone. Bottom right: MI-Based design for DJI-M100 drone.

CHAPTER 6:
Conclusions

6.1 Summary and Conclusions

In this work, we introduced a novel approach for a low-cost radar system design by integrating the MLRS-based receiver with matched illumination waveforms for specific targets. An algorithm to design a low-rate matched waveform was implemented for both SNR-based waveform and MI-based waveform that is optimal based on filter allocation constraint. To address the target ensemble large-angle deviation issue, the algorithm could produce a design for the unknown angle corresponding to a random target response as well as a known angle case corresponding to a deterministic target response.

In order to test our system performance with practical targets, we used the Naval Postgraduate School anechoic chamber to measure target responses of different drones. We took measurements at several angles and in several frequency bands. To extract a target impulse response from the raw measurements, we had to perform post-processing operations. First, we coherently integrated five thousand pulses to increase SNR; then we had to eliminate undesired signals which were reflected from the pedestal and possibly other surfaces. The undesired signals were reduced using background subtraction by taking two recordings; one with a target and one without a target. Each set of recordings was aligned in phase and scaled to have the same amplitude to get maximum reduction of the background signals. Lastly, after the measurement was integrated and cleaned from the background, we were left with the reflected signal from the target. This signal was a convolution of the transmit waveform, which was known, and the target impulse response, which we were trying to extract. To complete the post-processing, we performed a deconvolution operation to extract the target impulse response from the return signal. This process was repeated to obtain the targets responses for the different angles and frequency bands. This method allowed us to get a high-bandwidth complex-valued impulse response of a target in a specific angle.

The performance metric for the design was probability of detection. By using Monte Carlo simulations, we produced a probability of detection curve for a given set of waveform and

receiver design, transmit energy, and a target response. From the results, it was shown that the low-rate matched waveform design developed in this work outperformed wideband waveform in all cases, except for the case of the target ensemble with large angle deviation and with high transmit energy. We also found that SNR-based waveform performed better than MI-based waveform for all known target cases. For the same total bandwidth, it was beneficial to have more channels in terms of detection.

This design approach can be used as a building block for a future low-cost detection system. The design approach maintains the benefits of matched illumination waveform in terms of improved probability of detection and the use of low-rate sampling that can significantly reduce the cost of a system.

6.2 Future Work

Other than taking measurements of other targets and testing the robustness of the design, it will be worthwhile to demonstrate low bandwidth matched-illumination radar transmitter-receiver in a laboratory or a field experiment. The design reported in this work is suitable for a real-time hardware implementation and can be utilized using FPGA or a software defined radio (SDR). Previous studies [17]-[19] demonstrated multi-band SDR radar with traditional waveforms such as FMCW and LFM. The next step will be to incorporate matched illumination waveform in SDR or FPGA-based radar applications using the approach developed in this work.

List of References

[1] M. R. Bell, "Information theory and radar waveform design," *IEEE Trans. Inform. Theory*, vol. 39, no. 5, pp. 1578-1597, Sep. 1993.

[2] R. A. Romero, J. Bae and N. A. Goodman, "Theory and application of SNR and mutual information matched illumination waveforms," *IEEE Trans. Aero. and Elec. Sys.*, vol. 47, no. 2, pp. 912-926, Apr. 2011.

[3] R. A. Romero, "Detection performance of matched transmit waveform for moving extended targets,," *2013 Asilomar Conf. on Sig., Sys. and Computers.*, pp. 1956-1960, Nov. 2013.

[4] R. A. Romero, "Matched waveform design and adaptive beamsteering in cognitive radar applications," Ph.D. dissertation, Dept. of Elec. and Comp, Univ. of Arizona, USA, 2010.

[5] M. A. Richards, J. A. Scheer, and W. A. Holm, *Principles of Modern Radar: Basic principles, Volume 1: Basic principles*, Volume 1. Raleigh, NC, USA: SciTech Pub., 2010.

[6] P. E. Pace, "To See and Not To Be Seen," in *Detecting and Classifying Low Probability of Intercept Radar*, 2nd ed. Boston, MA, USA: Artech House, 2009, ch.1, pp. 3-37.

[7] Y. C. Eldar, and G. Kutyniok, "Introduction to compressed sensing," in *Compressed Sensing Theory and Applications*, Cambridge, MA, USA: Cambridge University Press, 2012, ch. 1, pp. 1-64.

[8] P. E. Pace, R. E. Leino, and D. Styer, "Wideband Undersampling Digital Receiver," U.S. Patent 6 031 879 , Feb. 29, 2000.

[9] M. Johnson, "Signal recovery and detection of certain wideaband signals using multiple low-rate ADCs," Thesis, Dept. of Elec. and Comp. Eng, Naval Postgraduate School, Monterey, CA, USA, 2018.

[10] M. Johnson and R. A. Romero, "Signal recovery and detection of certain wideaband signals using multiple low-rate ADCs," *2019 Aerospace Confrence*, Big Sky, MT, USA, 2019, pp. 1-9.

[11] M. Hamid, N. Bjorsell and S. Ben Slimane, "Signal bandwidth impact on maximum-minimum eigenvalue detection," *IEEE Communications Letters*, vol. 19, no. 3, pp. 395–98, 2015.

[12] P. M. Woodward, *Probability and Information Theory: With Applications To Radar*. New York, NY, USA: McGraw-Hill, ch.4, pp. 62–76, 1953.

[13] S. M. Kay, *Fundamentals of Statistical Signal Processing*. McGraw-Hill, Englewood Cliffs, NJ, USA: Prentice-Hall PTR, 1994.

[14] Q. J. O. Tan, R. A. Romero and D. C. Jenn, "Target recognition with adaptive waveforms in cognitive radar using practical target RCS responses," *2018 IEEE Radar Conf.*, Apr 2018, OKC, OK.

[15] C. J. Li and H. Ling, "An investigation on the radar signatures of small consumer drones," *IEEE Antennas Wirel. Propag. Lett.*, vol. 16, pp. 649–652, 2017.

[16] A. M. Morgan, "Ultra-wideband impulse scattering measurements," *in IEEE Transactions on Antennas and Propagation*, vol. 42, no. 6, pp. 840–846, Jun. 1994.

[17] Y. Kwag, J. Jung, I. Woo, and M. Park, "Multi-band multi-mode SDR radar platform," *in 2015 IEEE 5th Asia-Pacific Conference on Synthetic Aperture Radar (APSAR)*, Singapore, Sep. 2015, pp. 46–49.

[18] Y. Kwag and I. Woo, "Multi-band multi-mode SDR radar platform for traffic and security applications," *2016 URSI Asia-Pacific Radio Science Conference (URSI APRASC)*, Seoul, 2016, pp. 1182-1183

[19] Y. Kwag, I. Woo, H. Kwak and Y. Jung, "Multi-mode SDR radar platform for small air-vehicle Drone detection," *2016 CIE International Conference on Radar (RADAR)*, Guangzhou, 2016, pp. 1-4. doi: 10.1109/RADAR.2016.8059254

THIS PAGE INTENTIONALLY LEFT BLANK

Initial Distribution List

1. Defense Technical Information Center
   Ft. Belvoir, Virginia

2. Dudley Knox Library
   Naval Postgraduate School
   Monterey, California